Alpha localized radiolysis and corrosion mechanisms at the iron/water interface: Role of molecular species

Johan Vandenborre, F. Crumière, G. Blain, R. Essehli, Bernard Humbert, M. Fattahi

Alpha localized radiolysis and corrosion mechanisms at the iron/water interface: Role of molecular species.

Johan Vandenborre*[1], Francis Crumière[1], Guillaume Blain[1], Rachid Essehli[1], Bernard Humbert[2], Massoud Fattahi[1]

1 SUBATECH, Unité Mixte de Recherche 6457, Ecole des Mines de Nantes, CNRS/IN2P3, Université de Nantes, 4 rue Alfred Kastler, BP 20722, 44307 Nantes cedex 03, France.

2 Institut des Matériaux Jean Rouxel, Université de Nantes, CNRS, 2 rue de la Houssinière, BP 32229, 44340 Nantes, France

* To whom correspondence should be addressed:

E-mail: johan.vandenborre@subatech.in2p3.fr.

Address: SUBATECH, Unité Mixte de Recherche 6457, Ecole des Mines de Nantes, CNRS/IN2P3, Université de Nantes, 4 rue Alfred Kastler, BP 20722, 44307 Nantes cedex 03, France.

Phone (+33) 251 858 536

Fax (+33) 251 858 452

Abstract

This paper is devoted to the iron corrosion phenomena induced by the α ($^4He^{2+}$) water radiolysis species studied in conjunction with the production/consumption of H_2 at the solid/solution interface. On one hand, the solid surface is characterized during the $^4He^{2+}$ ions irradiation by *in situ* Raman spectroscopy; on another hand, the H_2 gas produced by the water radiolysis is monitored by *ex situ* gas measurements. The $^4He^{2+}$ ions irradiation experiments are provided either by the CEMHTI (E = 5.0 MeV) either by the ARRONAX (E = 64.7 MeV) cyclotron facilities. The iron corrosion occurs only under irradiation and can be slowed down by H_2 reductive atmosphere. Pure iron and carbon steel solids are studied in order to show two distinct behaviors of these surfaces *vs.* the $^4He^{2+}$ ions water irradiation: the corrosion products identified are the magnetite phase ($Fe(II)Fe(III)_2O_4$) correlated to an H_2 consumption for pure iron and the lepidocrocite phase (γ-Fe(III)OOH) correlated to an H_2 production for carbon steel sample. This paper underlined the correlation between the iron corrosion products formation onto the solid surface and the H_2 production/consumption mechanisms. H_2O_2 species is considered as the single water radiolytic species involved into the corrosion reaction at the solid surface with an essential role in the oxidation reaction of the iron surface. We propose to bring some light to these mechanisms, in particular the H_2 and H_2O_2 roles, by the *in situ* Raman spectroscopy during and after the $^4He^{2+}$ ions beam irradiation. This *in situ* experiment avoids the evolution of the solid surface, in particular phases which are reactive to the oxidation processing.

Keyword: Iron Corrosion Products, $^4He^{2+}$ Irradiation, Water Radiolysis, *In situ* Raman Spectroscopy, Radiolytic Molecular Species.

1. Introduction

In the specific actual context of the nuclear power plants using by any countries, the study of iron based materials, implied in the most of the nuclear industry buildings, seems relevant [1]. In this aim, the iron based materials have been studied under pure iron [2, 3], low alloy and stainless steel [1, 4, 5] regarding the using ever in the nuclear reactors, in the radioactive waste transport or storage/disposal.

Disregarding the high number of publications about the corrosion of these materials with [2-10] or without [11-14] irradiation, the combination of iron corrosion and water radiolysis mechanisms have not sufficiently been investigated in order to understand the part of each chemical processing. Moreover, much papers deal with the iron corrosion products under atmospheric conditions [2, 3, 11], anoxic [6, 15] or both [4] and a few of them under nuclear reactors conditions [5, 7, 16]. These works have performed characterization of the iron corrosion products with different spectroscopic tools such as Raman vibrational spectroscopy by *in situ* [12] or *ex situ* [14, 15, 17-20] experiments. These works show that the main corrosion products at the iron based materials surface are magnetite (Fe_3O_4), hematite (α-Fe_2O_3), maghemite (γ-Fe_2O_3), goethite (α-FeOOH) and lepidocrocite (γ-FeOOH) *versus* the experimental conditions (pH, potential, temperature, contact duration). Moreover, the intermediate phase called "green rust" is detected and characterized onto the iron based materials surface [12, 13]. The production of these green rust phases, clearly identified by Raman spectroscopy since 1996 by studies coupling Mossbauer and Raman spectroscopy on mineralogic samples [21], are induced by potential, pH parameters and the Fe(III)/Fe(II) ratio at the solid surface [13]. The *in situ* experiment, such Raman spectroscopy, is able to monitoring the formation of theses corrosion products which can induce specific properties to the solid surface such as electronic transfers between solution and surface [12].

The α ($^4He^{2+}$) radiolysis of water mainly induces molecular species such as H_2 and H_2O_2 [16,

22-24]. The hydrogen gas produced by the water radiolysis, in particular at the solid/solution interface in the case of Fe [2, 4, 5], Zr [25-27], Si [28-30], Ti [31], Ce [26, 27] or U [27] oxides could be considered as one possible relevant future source of energy and then consists as a new field of fundamental investigations. Most the pre-quoted works systems oxides/water has shown an increase of the H_2 radiolytic yield regarding the pure water system. Few proposed mechanisms can be involved in the enhancement of hydrogen production by irradiation at the solid surface: (i) the hydrogen enrichment of the solid surface implying the $H^+(H_2O)$ cluster formation [2, 3], (ii) the electron-hole pair formation and exciton migration induced by the solid irradiation [3, 26-28, 30-34], (iii) the role of hydroxyl groups density onto the solid surface [28, 29, 32, 35]. The oxidative species H_2O_2, produced by chemical surface decomposition mechanism [25-27, 36, 37], has been described as the main source to produce hydroxyl groups at the solid surface. The irradiation consequences onto the iron based materials corrosion are largely studied with different experimental conditions. The irradiation experiments are performed with different devices which provide irradiations with γ [4-10, 25-30, 33-35, 38], neutrons [5-7], β(electrons) [28, 32] or α ($^4He^{2+}$) [26, 27, 33] and protons [2, 3] in specific ion beam fluence conditions. Thus, in the most of studies, the water volume irradiated is not accurately controlled: either whole of the system is irradiated (typically γ, neutrons and electrons irradiations) or the solid with any water layers sorbed onto its surface. Moreover, for example for H_2O_2 species, the radiolytic yield determination depends on the LET (Linear Energy Transfer = stopping power = –dE/dx) and the spatial distribution of the dose during the ion beam irradiation [36]. Consequently, the corrosion mechanisms have not been completely decorrelated from the water radiolysis mechanisms. The mechanisms of corrosion induced by the $^4He^{2+}$ water radiolysis are not clearly defined. Therefore, this paper proposes an experiment of localized radiolysis of water by the $^4He^{2+}$ ions irradiation in contact with the solid studied in order to understand the effect of the

radiolysis molecular species (H_2 and H_2O_2) onto the iron based materials corrosion mechanisms.

2. Material and methods

Table 1 gives details about experiment sets and irradiation runs that are performed in this work. The influence of the following parameters is studied: 1) solids samples (pure iron or carbon alloy steel), 2) atmosphere (aerated, Ar or Ar/H_2), 3) irradiation conditions ($^4He^{2+}$ ion energy, dose, irradiation time and dose rate), 4) Hydrogen peroxide source which is coming either from water radiolysis either from manual addition. In this aim we have performed measurements into solution, gas and solid in order to analyze radiolysis products and their effects onto the solid surface during and/or after irradiation. For the sets II and III, the experiments are repeated in order to measure the solution immediately after the irradiation and the solids analysis 48 hours after the irradiation (sets II' and III'). Thus, solids characterization experiments are separated in two ways: for the *in situ* experiments (sets IV, VII, VIII) the measurements are performed during and after irradiation in the same cell onto the $^4He^{2+}$ beam line with Raman spectroscopy while in the *ex situ* experiments (sets II, III, V, VI) the solids are put off the beam line and analyzed by XPS and Raman spectroscopy.

2. 1 Systems

Ultrapure water (Millipore Alpha-Q with an electrical resistivity of 18.2 MΩ) is used in the whole of our study. The solid samples are in contact with it during the total experiment time of 15 h.

Two iron based materials are chosen: (1) pure iron sample to understand the chemical mechanisms and (2) carbon alloy steel used in the nuclear industry. Pure iron is purchased by GOODFELLOW with a high purity (99.9 %). The normalized carbon alloy steel sample is P235GH that is used in the nuclear industry into pressure vessels, boilers and heat exchangers

(For the chemical composition see Table 2). The solids samples are cut into 10×10×1 mm and polished down to a surface roughness of 3 µm with a Buehler polisher and cleaned in a HCl (15 %) + $NaCO_3$ (5 %) solution. Before performing the experiments, the solid samples are etched by ions Ar^+ (5 kV during 10 min) into the XPS apparatus as detailed below in order to eliminate iron oxidation products at the surface. During all the process (etching, transport, storage), the samples are preserved from oxidation by an inert atmosphere in N_2 glove box and Ar transport into irradiation cells. All the experiments are performed at a temperature of 298 K.

2. 2 Irradiations

$^4He^{2+}$ ions irradiations are provided by the CEMHTI cyclotron facility (Orléans, France) onto a horizontal beam-line and by the ARRONAX cyclotron facility (Saint-Herblain, France) onto a vertical beam-line. The use of both cyclotrons allows us to explore a wide range of energy and LET values. The CEMHTI cyclotron generates $^4He^{2+}$ particles beams with energies of 28 MeV while the ARRONAX cyclotron reaches a 68 MeV energy. The energy of the $^4He^{2+}$ particles inside the irradiation cell is systematically evaluated by using the SRIM 2008 simulation code [39, 40], where the whole of the obstacles upstream of the cell is taken into account. The irradiation cell, made from PEEK polymer with 20 mL of the solution under continuous stirring, is equipped with a borosilicate glass disc as entrance window (Diameter = 25 mm, Thickness = 150 ± 10 µm) with an electrolyte thickness between it and the solid sample of 5 mm. During the irradiation runs, the cell is closed and has been checked that it does not produce H_2. The computations establish that the range of the $^4He^{2+}$ ion energy varies from 5.0 MeV for CEMHTI facility (Average LET = 151.5 keV/µm) to 64.7 MeV for ARRONAX one (Average LET = 22.7 keV/µm). Providing by the CEMHTI cyclotron, the flux of $^4He^{2+}$ particles within the irradiation cell is measured with a Faraday cup and set to 10 nA depending on the experiment. The stability of the $^4He^{2+}$ ions beam is checked by

monitoring the beam current set down in an ionization chamber (measured at 40 nA) located upstream to the irradiation cell. Other experiments are carried out within ARRONAX cyclotron at 64.7 MeV. The intensity of the particles beam, measured on an internal Faraday cup located one meter upstream, is maintained at 70 nA. The uncertainty of that current measurement is of 10 %. Fricke dosimetry [41] is used in this study in order to determine the dose into the samples. This method is based on the oxidation of Fe^{2+} to Fe^{3+} by the species produced by the water radiolysis reactions. The concentration of ferric ions is monitored by UV-Vis measurements at 304 nm (ε = 2197 $L.mol^{-1}.cm^{-1}$, 298 K) with a spectrophotometer CARY4000 (VARIAN). These measurements are carried out on samplings few minutes after irradiation. Super Fricke solutions are prepared by dissolving the desired quantity of Mohr's salt ($[Fe^{2+}]$ = 10 $mmol.L^{-1}$) and NaCl (1 $mmol.L^{-1}$) in aerated aqueous 0.4 $mol.L^{-1}$ H_2SO_4 solutions. All reagents are analytical grade or equivalent. NaCl is added in order to avoid any organic impurities. The irradiation time is 3 min for ARRONAX experiments and either 15 min or 120 min for CEMHTI experiments, according to the desired irradiation dose. By the Fricke dosimeter, the dose rates are measured respectively at 80 $Gy.min^{-1}$ and 7500 $Gy.min^{-1}$ during irradiation in CEMHTI and ARRONAX facilities using the ferric ion radiolytic yield extrapolated from the literature [42-44] ($G(Fe^{3+})$ = 5.0 10^{-7} $mol.J^{-1}$ for E = 5.0 MeV and $G(Fe^{3+})$ = 11.7 10^{-7} $mol.J^{-1}$ for E = 64.7 MeV).

2.3 Molecular species measurements (H_2, H_2O_2)

The H_2O_2 addition experiment, instead of the $^4He^{2+}$ irradiation, is carried out by adding the H_2O_2 solution at a volumic concentration, close to its measured in the previous experiment (set I), into the carbon steel/ultrapure water system for the same time than the ARRONAX irradiation experiment. The concentrations of H_2O_2 have been determined, about 15 min after the experiment, with the Ghormley triiodide method [45] using two reagents. One is a mixture of ammonium molybdate ($Mo_7O_{24}(NH_4).2H_2O$, Carlo Erba), potassium iodide (KI, VWR) and

sodium hydroxide (NaOH, VWR) and the second is a buffer solution (pH 4-5) of acid potassium phthalate ($C_8H_5KO_4$, VWR). For a total volume of 2 mL, 500 µL of both reagents are mixed with 1 mL of the sample solution. The concentration of H_2O_2 is obtained indirectly by measurement of I_3^- absorbance with the UV-VIS spectrophotometer CARY4000 (VARIAN). The molar extinction coefficient of I_3^- at the 351 nm wavelength is previously determined at 25300 $L.mol^{-1}.cm^{-1}$ in the studied solution at 298 K.

Molecular hydrogen is measured with a gas chromatograph. Ultra high purity argon is used as the carrier gas with a pressure of 150 kPa. The gas chromatograph is a 490-GC, which is a µ-GC model from VARIAN. The gas sample is introduced using a Swagelok connection and the injection volume is 10 µl. The column is a Molecular Sieve 5A (length = 4 m and diameter = 0.25 mm). The detection is performed using a thermal conductivity detector. Calibration of the detector is performed by injection of different gas mixture of Argon/Hydrogen from 10 to 500 ppm of hydrogen in the composition of the gas. Uncertainty in gas measurements is estimated to be less than 10 %.

2.4 Solid phase characterization.

Solid analysis are performed by *ex situ* and *in situ* experiments: 1) *ex situ* experiments are carried out by XPS (X-ray photoelectron spectroscopy) and Raman spectroscopy after irradiation runs, 2) *in situ* experiment is carried out during the irradiation into the ARRONAX cyclotron facility by Raman spectroscopy as detailed in the following section.

The $Fe_{2p3/2-1/2}$ XPS spectra are collected by an XPS apparatus with a KRATOS AXIS ULTRA electron spectrometer working in fixed analyzer transmission (FAT) mode. The source of photons is an Al monochromatic X-ray source emitting an incident X-ray beam at 1486.7 eV with a FWHM (full-width half-maximum) of 0.25 eV. The sample, fixed on a metallic plate, is analyzed in a chamber under 5 10^{-7} Pa vacuum. The $Fe_{2p3/2-1/2}$ peaks are recorded at constant pass energy of 20 eV. The charge effects are corrected using the C1s line of the

carbon at 284.7 eV. The angle-resolved XPS spectra are fitted using a Gaussian–Lorentzian peak shape with a Shirley baseline as background. The binding energy precision is better than 0.2 eV.

All the Raman system is purchased by the HORIBA Jobin-Yvon Company. Raman spectra are recorded with an iHR550 spectrometer equipped with two optic fibers (diameter = 100 µm, length = 20 m). The detector is a charged coupled device (CCD) cooled by Peltier effect (203 K). Raman spectra are excited with a laser beam at 632.8 nm emitted by a He/Ne Laser. The laser beam is weakly focused on samples with a diameter of about 1 mm and a power of about 14 mW for a working distance of 40 mm on the sample and an acquisition time of 2 minutes. The Raman backscattering is collected through an objective system and dispersed by 1200 groves/mm gratings to obtain 5 cm^{-1} spectral resolution for Raman stokes spectra excited at 632.8 nm. The wavenumber accuracy is checked and considered better than 0.5 cm^{-1}.

With the Raman spectroscopic device (laser excitation and back scattering Raman) described before, *in situ* experiments have been performed onto the solid samples in contact with ultrapure water. Figure 1 displays the device installed onto the $^4He^{2+}$ beam line. The $^4He^{2+}$ ions beam is provided by the ARRONAX cyclotron facility with E = 64.7 MeV. The average length of the $^4He^{2+}$ particle for this energy is determined at about 2.5 mm in the ultrapure water solution by the SRIM 2008 simulation code [39, 40]. Thus, we have checked experimentally that for a volume solution of 2 mL, volume of the irradiation cell onto the ARRONAX beam line, with a solid/$^4He^{2+}$-beam distance of 5 mm, the $^4He^{2+}$ ions irradiation direct effects occur onto the solution and not onto the solid surface. So, with this *in situ* experimental device experiment under irradiation, this paper is devoted to study the effect of the water radiolysis species onto the solid corrosion and not the direct irradiation consequences onto the solid surface.

3. Results

The irradiation runs are carried out onto the CEMHTI cyclotron facility (E = 5.0 MeV, Dose Rate = 80 $Gy.min^{-1}$) in order to follow the phases formation onto the two solid surfaces induced by the water radiolysis species. All the experimental conditions of the irradiation runs are described in Table 1. Then, we study the sets I, II and III (pure water, iron and carbon steel solid systems respectively).

3.1 Solid *ex situ* characterization

So, the first experiments are the solid characterization after the irradiation (*ex situ*) by XPS and Raman spectroscopy. Figures 2 and 3 present respectively the Raman and the XPS results onto the sets II and III of the samples after the irradiation. Under these deaerated conditions, the Raman spectra dominated by a specific band at 670 cm^{-1}, are assigned to the magnetite $Fe(II)Fe(III)_2O_4$ as shown by many authors [8, 10, 12, 15, 19, 20, 46] in agreement with the black color phase induced by the water radiolysis species onto the iron sample (set II). Onto the carbon steel sample (set III), we observe the vibrational Raman bands at 250/380/530/660 cm^{-1} assigned to the lepidocrocite γ-Fe(III)OOH orange color phase [8, 14, 46-49]. For XPS experiments, we have taken care about the inert atmosphere during the transport of sample between the cyclotron facilities and the XPS device in order to avoid the oxidation of the samples. The XPS spectra, displayed in Figure 3 with the fitting parameters described into Table 3, show that the results of the Ar^+ etching is characterized by a Fe2p spectrum where the iron element is only under the Fe(0) form (BE = 706.3 eV) for the two solid surfaces (same spectrum for the two samples). This alone peak assigned to the Fe(0) let us to assume that the etching process is efficient to eliminate other secondary phases which are commonly observed onto the iron based materials. Other XPS spectra of sets II and III corroborate the results previously determined by the Raman measurements. Indeed, the Fe(III) component (BE = 711.3 eV) found onto the carbon steel sample (set III) and the Fe(II)/Fe(III)

components (respectively BE = 709.0/711.3 eV) found onto the iron surface (set II) are induced only by the water radiolysis species provided by the $^{4}He^{2+}$ beam irradiation. These results corroborate the formation of a Fe(III) oxide phase for the carbon steel sample and a Fe(III)/Fe(II) mixed oxide for the iron one during the irradiation experiments for these deaerated conditions. We have performed experiments in the same conditions but without irradiation (sets V and VI). The solid characterization by XPS and Raman spectroscopy do not reveal any Fe(III) and/or Fe(II) species onto the iron and carbon steel samples. Then, the magnetite and lepidocrocite phases are produced only by the radiolysis species reactions onto the solids surface.

3.2 Radiolytic molecular species measurements (H_2, H_2O_2)

The aim of the second experiment is to understand the role of specific radiolysis species created during the water irradiation and that can react with the solid surface, *i.e.*, H_2 and H_2O_2. We have repeated the irradiation experiments in the same conditions but with a lower duration and obviously a lower dose into the solution in order to avoid highest hydrogen concentration into the irradiation cell. The concentrations of these species after the irradiation monitored by µ-GC and Ghormley triiodide method [45] are presented in Table 4. The H_2 concentration measurements show the difference between the iron sample (set II) and the carbon steel sample (set III). Although the consumption of H_2 by the iron surface vs. the pure water system (from $[H_2] = 1.0\ 10^{-4}$ mol.L^{-1} to $[H_2] = 0.3\ 10^{-4}$ mol.L^{-1}) is clearly measured; the carbon steel surface have produced a non-negligible part of H_2 ($[H_2] = 1.6\ 10^{-4}$ mol.L^{-1}). Thus, the production of magnetite and the lepidocrocite phases have to be related respectively to the H_2 production/consumption reactions. Moreover, the H_2O_2 concentrations seem to show a low consumption of this species induced by the $^{4}He^{2+}$ radiolysis by the both solids (respectively from initial concentration of $7.1\ 10^{-5}$ mol.L^{-1} in the pure water to an average concentration of $[H_2O_2] = 6.1\ 10^{-5}$ mol.L^{-1} in contact with solids). Then, the reaction kinetic seems much lower

than for the other molecular radiolytic species such as H_2.

3.3 *In situ* Raman experiment

The second $^4He^{2+}$ ions irradiation runs in this work are performed into the ARRONAX cyclotron facility which provides a higher energetic $^4He^{2+}$ beam (E = 64.7 MeV, Dose Rate = 7.5 kGy.min^{-1}) coupled with the *in situ* Raman experiment as described in the Experimental section. Moreover, with this device, the carbon steel sample has been followed, for a long time (15 hours) during and after the irradiation. By this way, we have checked that the previously observed phases come from the radiolytic species and not from another parasite reactions such as the oxidation by the atmosphere after experiments. Moreover, this experiment allows us to access to the kinetic of these formation reactions. The experimental samples for sets IV and VII have been performed with the same experimental conditions: the water irradiation by the ARRONAX $^4He^{2+}$ beam during a short time (3 minutes), continuously *in situ* analyzed by Raman spectroscopy during a long time (15 h) onto the beam line. The difference between the sets IV and VII is the attendance or not of the borosilicate glass disc as entrance window (Diameter = 25 mm, Thickness = 150 µm). While the set VII (with borosilicate glass disc) the atmosphere into the cell is Ar/H_2, with H_2 produced by the water radiolysis, the set IV experiment (without borosilicate glass disc) is performed under aerated conditions. For instance, Raman spectra of set IV *vs.* time are presented in the Figure 4**.**

On the one hand, the Raman band at 885 cm^{-1}, assigned to the H_2O_2 species detected into the solution, is present during all the experiment duration. So this *in situ* Raman experiment confirms the assumption that the H_2O_2 species can interact with the solid surface. For the last spectrum recorded, the Raman vibrational bands of lepidocrocite characterized by 250/380/530/660 cm^{-1} as onto the previous experiment III is displayed.

On the other hand, the *in situ* Raman spectra of the set VII (carbon steel sample and Ar/H_2 atmosphere) does not show the occurrence of corrosion phase: Any corrosion process does not

occur under this reductive atmosphere by the H_2 effect at the time scale of this experiment.

Finally, in order to specify the H_2O_2 role into the corrosion process, we have repeated in the set VIII the *in situ* Raman experiment under aerated conditions but with an H_2O_2 addition with a volumic concentration close to it previously determined in the experiment I ($[H_2O_2]$ = 1.0 10^{-4} mol.L^{-1}) instead of the previous described $^4He^{2+}$ ions irradiation (set IV). The Raman measurements display exactly the same corrosion phase formation onto the carbon steel surface with the Raman measurements. Thus, H_2O_2 species can be considered as the single radiolytic species which induces corrosion process in our system of $^4He^{2+}$ water localized radiolysis. However, the experiment is performed under aerated conditions, so we can not exclude the dissolved O_2 species role ($[O_2]$ = 3.7 10^{-4} mol.L^{-1}) into the corrosion process.

Results are obtained onto the different experiments (set I to VIII). The $^4He^{2+}$ ions irradiation of water, under desaerated and non reductive conditions, induces an iron based material corrosion with two cases: i) onto the carbon steel sample surface, the lepidocrocite phase formation with H_2 production; ii) onto the pure iron sample surface, the magnetite phase formation with H_2 consumption. Moreover, H_2O_2 radiolytic species occurs in the same way for the both phases formation and is considered as the single radiolytic species implied into the iron based material corrosion process.

4. Discussion

On the basis of these results we will propose now an iron based material corrosion mechanisms under the $^4He^{2+}$ ions irradiation presented by Figure 5.

4.1 Part A: Water Radiolysis

The water radiolysis has been extensively studied and described in the literature regardless the experimental conditions [22-24]. The radiolytic species induced are either radicals (°OH, e^-_{aq}, °H) or molecular species (H_3O^+, H_2O_2, H_2). Let us notice that the radicals species are

considered as so much reactive and then with a very short distance into the irradiated solution when the LET value of radiation is above 20 keV/µm as underlined by the literature [50]. Therefore, in our experimental conditions (solution volume *vs.* $^4He^{2+}$ particles average length) described in the Experimental section, the solids can not be irradiated by the $^4He^{2+}$ particles beam regardless the cyclotron facility used. Therefore, only the molecules species, in particular H_2O_2 and H_2, will be considered here.

4.2 Parts B and C: H_2O_2 surface decomposition and Lepidocrocite Formation/H_2 production

The lepidocrocite formation induced by the solid oxidation, observed in this work for the set III (carbon steel sample), occurs by the H_2O_2 molecule into the irradiated solution with a non negligible concentration (about 7 10^{-5} mol.L^{-1}). This lepidocrocite formation has been described by authors with three steps: 1) the catalytic decomposition of H_2O_2 onto the solid surface [4, 11, 26, 27, 33, 37, 38, 51] (reaction 1) with formation of O_2 or °OH according to the surface properties and the pH values of the solution [37, 38, 51], 2) the Fe oxidation by the O_2 or °OH species (reaction 2) with iron(II) hydroxide $Fe(OH)_2$ formation [4, 11] similar to the U(IV) oxidation displayed in a previous study [37], 3) the oxidation of this iron hydroxide by the H_2O_2 species in order to create the lepidocrocite γ-Fe(III)OOH structure [4, 11, 13] (reaction 3) identified in our work by XPS and Raman spectroscopy.

$H_2O_2 \rightarrow H_2O + 1/2\ O_2$ or 2 °OH (1)

$2\ Fe + O_2 + 2\ H_2O \rightarrow 2\ Fe(OH)_2$ (2)

$2\ Fe(OH)_2 + H_2O_2 \rightarrow 2\ FeOOH + 2\ H_2O$ (3)

Any authors [50] have observed that H_2 addition have no effect onto the H_2O_2 production, but the H_2 species can be involved into the neutralisation of hydroxyl radicals species at the solid surface. This way is a possible explanation for our results obtained with the experimental set VII where the carbon steel solid corrosion is inhibited by the H_2 radiolytic species. Moreover,

the lepidocrocite formation does not depend on the LET values since it has been observed for a high range of $^{4}He^{2+}$ particle beam properties (5.0 MeV < E < 64.7 MeV, 151.5 keV/µm > LET > 22.7 keV/µm). For these highest LET values, it is underlined in a previous study [50] that radical species can not escape into the bulk solution. This result is consistent with the fact that only the molecular oxidative species H_2O_2 which is the main character into the lepidocrocite formation.

Both studies [37, 52], performed onto the UO_2 solids, assume that H_2O_2 is the single oxidative radiolytic species. So, in our work, we have checked that the H_2O_2 species can explain alone the iron corrosion process onto the samples surface as determined during the experiment onto the set VIII because the lepidocrocite phase formation is obtained either by H_2O_2 from the $^{4}He^{2+}$ water radiolysis either by the manual addition with a similar volumic concentration (1.0 10^{-4} mol.L^{-1}). Moreover, our results made the evidence that H_2O_2 species have been weakly consumed by the reaction with the carbon steel surface. Then, the H_2O_2 concentration induced by the $^{4}He^{2+}$ water radiolysis can be considered as sufficiently high to be involved into the chemical mechanisms proposed by Figure 5.

4.3 Part D: Magnetite Formation/H_2 consumption

During the experiment with the pure iron sample, the lepidocrocite formation is not the final chemical reaction at the surface. It has been underlined by many authors [11-13] the partial auto-reduction of Fe(III)OOH into the magnetite $Fe(II)Fe(III)_2O_4$ phase. Moreover, these authors considered this dissolution/precipitation reaction as irreversible (reaction 4).

$$\mathbf{3\ FeOOH + H_3O^+ + e^- \rightarrow Fe_3O_4 + 3\ H_2O\ (4)}$$

These results are in agreement with the literature where is presented the γ-irradiation-which induces the chemical change from the α-FeOOH and β-FeOOH to the magnetite phase [53]. The pure iron solid characterization has shown the occurrence of the magnetite phase by XPS and Raman spectroscopy. However, in our study, the magnetite phase formation is followed

by a non negligible H_2 consumption (about 60 % of the initial H_2 produced by the water radiolysis). Many assumptions can be considered:

1) An explanation has been given [30] where the authors propose a reaction between the H_2 species and the hole created by the exciton ejection at the solid surface during the irradiation. However, the exciton described in the literature [25-27, 30, 31, 38] is induced by the direct irradiation of the solid, while in our work it is not realistic. Indeed, we have underlined in the experimental section that in our work the solid sample is not directly irradiated.

2) Other authors [28] propose the possibility to depleted the H_2 species by the radical hydroxyl species during the surface irradiation (reactions 5 and 6). In previous studies [37, 38], it is validated that the H_2O_2 decomposition onto the solid surface can produce the radical hydroxyl species.

$^\circ OH + H_2 \rightarrow {}^\circ H + H_2O$ (5)

$^\circ H + H_2O_2 \rightarrow {}^\circ OH + H_2O$ (6)

3) Also, we propose that the H_2 consumption is directly linked to the magnetite phase occurrence as proposed in another study [12]. Therefore, we assume that the Fe(III) species in solution can be reduced by a part of the H_2 species which come from the water radiolysis. Particularly, in the case of the pure iron surface where no other redox reactions can occur on the contrary of the low carbon alloy steel surface where the C atoms or other impurities (cf Table 2) can disturb these Fe(III) reduction mechanisms. Then, the Fe(III) reduction into Fe(II) can explain the magnetite phase formation/precipitation at the iron surface and the H_2 radiolytic product consumption. Moreover, this last assumption seems realistic in our case because it can explain the strong difference of the H_2 concentration values between the carbon steel and the pure iron samples (respectively experimental set II and III) *vs.* the pure water system (set I).

However these assumptions need be confirmed/infirmed by further investigations in order to

describe the redox reactions at the iron and carbon alloy steel surfaces.

5. Conclusion

This work gives some insights on the $^{4}He^{2+}$ water radiolysis consequences onto the iron corrosion surface. In this way, we have chosen to monitor only the molecular radiolytic species with a localized irradiation into the solution and not onto the solid surface. That is the reason why we have performed an *in situ* Raman experiment during the irradiation which avoids other parasite reactions such as oxidation by the atmosphere. First conclusion is the iron corrosion occurs only under irradiation and can be slowed down by an H_2 reductive atmosphere. Moreover, we have studied pure iron and carbon steel solids in order to show two distinct behaviors of these surfaces *vs.* the $^{4}He^{2+}$ water irradiation: 1) For pure iron, the corrosion products identified is the magnetite phase ($Fe(II)Fe(III)_2O_4$) with a non negligible H_2 consumption; 2) For carbon steel sample, the corrosion products identified is the lepidocrocite phase (γ-Fe(III)OOH) with a higher H_2 production *vs.* the H_2 production into the pure water system. Thus, we are able to propose chemical mechanisms, from water radiolysis to the corrosion products formation onto the iron surfaces, under helium ions radiation chemistry influence with the lepidocrocite phase considered as an intermediate phase before the magnetite formation. Therefore, we have underlined the role of the iron corrosion products formation onto the H_2 production/consumption mechanisms. Finally, considering this work determined that the H_2O_2 species are the essential water radiolytic species involved into the corrosion reaction at the solid surface with an essential role in the oxidation reaction of the iron surface.

Acknowledgements

The authors acknowledge financial support by the French Agence Nationale de Recherche, ANR, in the project CISSRAD ALPHA and by the Région Pays de Loire. We acknowledge V. Fernandez and J.Y. Mevellec from the IMN laboratory for letting us perform XPS and support for Raman measurements. Finally, the authors acknowledge ARRONAX and CEMHTI staffs for the efficient performing of irradiation runs onto the cyclotron facilities.

References

[1] F. Cattant, D. Crusset, D. Féron, Corrosion issues in nuclear industry today, Materials Today, 11 (2008) 32-37.
[2] S. Lapuerta, N. Millard-Pinard, N. Moncoffre, N. Bérerd, H. Jaffrezic, G. Brunel, D. Crusset, T. Mennecart, Origin of the hydrogen involved in iron corrosion under irradiation, Surface and Coatings Technology, 201 (2007) 8197-8201.
[3] S. Lapuerta, N. Moncoffre, N. Bérerd, H. Jaffrezic, N. Millard-Pinard, D. Crusset, Ion beam analysis of the effect of O_2 and H_2O on the oxidation of iron under irradiation, Nuclear Instruments and Methods in Physics Research Section B: Beam Interactions with Materials and Atoms, 249 (2006) 470-473.
[4] W.G. Burns, W.R. Marsh, W.S. Walters, The g irradiation-enhanced corrosion of stainless and mild steels by water in the presence of air, argon and hydrogen, Radiation Physics and Chemistry (1977), 21 (1983) 259-279.
[5] H. Christensen, Effect of water radiolysis on corrosion in nuclear reactors, Radiation Physics and Chemistry (1977), 18 (1981) 147-158.
[6] M. Dos Santos Afonso, C.D. Di Risio, A. Roitberg, R.O. Marqués, M.A. Blesa, Reductive dissolution of neutron- and g-irradiated magnetite, International Journal of Radiation Applications and Instrumentation. Part C. Radiation Physics and Chemistry, 36 (1990) 457-460.
[7] I. Teodorescu, I. Zberea, Influence of reactor irradiation on surface corrosion of pure iron, Journal of Nuclear Materials, 24 (1967) 347-349.
[8] V. Čuba, J. Indrei, V. Múčka, M. Nikl, A. Beitlerová, M. Pospíšil, I. Jakubec, Radiolytic formation of ferrous and ferric ions in carbon steel - deaerated water system, Radiation Physics and Chemistry, 80 (2011) 440-445.
[9] K. Daub, X. Zhang, J.J. Noël, J.C. Wren, Effects of γ-radiation versus H_2O_2 on carbon steel corrosion, Electrochimica Acta, 55 (2012) 2767-2776.
[10] N.R. Smart, A.P. Rance, L.O. Werme, The effect of radiation on the anaerobic corrosion of steel, Journal of Nuclear Materials, 379 (2008) 97-104.
[11] S. Hoerlé, F. Mazaudier, P. Dillmann, G. Santarini, Advances in understanding atmospheric corrosion of iron. II. Mechanistic modelling of wet-dry cycles, Corrosion Science, 46 (2004) 1431-1465.
[12] K. Ritter, M.S. Odziemkowski, R.W. Gillham, An in situ study of the role of surface films on granular iron in the permeable iron wall technology, Journal of Contaminant Hydrology, 55 (2002) 87-111.
[13] C. Ruby, A. Géhin, R. Aissa, J.M.R. Génin, Mass-balance and Eh-pH diagrams of FeII-III green rust in aqueous sulphated solution, Corrosion Science, 48 (2006) 3824-3837.
[14] D. Neff, L. Bellot-Guerlet, P. Dillmann, S. Réguer, L. Legrand, Raman imaging of ancient rust scales on archaeological iron artefacts for long-term atmospheric corrosion mechanisms study, Journal of Raman Spectroscopy, 37 (2006) 1228-1237.
[15] A. Puranen, M. Jonsson, R. Dähn, D. Cui, Immobilization of selenate by iron in aqueous solution under anoxic conditions and the influence of uranyl, Journal of Nuclear Materials, 392 (2009) 519-524.
[16] H. Christensen, S. Sunder, Current state of knowledge of water radiolysis effects on spent nuclear fuel corrosion, Anglais, 131 (2000) 102-123.
[17] H. Aubriet, B. Humbert, M. Perdicakis, Interaction of U(VI) with pyrite galena and their mixtures a theoretical and multitechnique approach Radiochimica Acta, 94 (2006) 657-663.

[18] D.L.A. De Faria, F.N. Lopes, Heated goethite and natural hematite: Can Raman spectroscopy be used to differentiate them?, Vibrational Spectroscopy, 45 (2007) 117-121.
[19] M.A. Legodi, D. de Waal, The preparation of magnetite, goethite, hematite and maghemite of pigment quality from mill scale iron waste, Dyes and Pigments, 74 (2007) 161-168.
[20] D. Neff, P. Dillmann, L. Bellot-Gurlet, G. Beranger, Corrosion of iron archaeological artefacts in soil: characterisation of the corrosion system, Corrosion Science, 47 (2005) 515-535.
[21] F. Trolard, J.M.R. Génin, M. Abdelmoula, G. Bourrié, B. Humbert, A. Herbillon, Identification of a green rust mineral in a reductomorphic soil by Mossbauer and Raman spectroscopies, Geochimica et Cosmochimica Acta, 61 (1997) 1107-1111.
[22] A.O. Allen, The radiation chemistry of water and aqueous solutions, Princeton, USA, 1961.
[23] Z.D. Draganic, I.G. Draganic, The Radiation Chemistry of Water, New York, USA, 1971.
[24] C. Ferradini, J. Pucheault, Biologie de l'action des rayonnements ionisants, Masson, Paris, France, 1983.
[25] J.A. LaVerne, H_2 Formation from the Radiolysis of Liquid Water with Zirconia, The Journal of Physical Chemistry B, 109 (2005) 5395-5397.
[26] J.A. LaVerne, L. Tandon, H_2 Production in the Radiolysis of Water on CeO_2 and ZrO_2, The Journal of Physical Chemistry B, 106 (2002) 380-386.
[27] J.A. LaVerne, L. Tandon, H_2 Production in the Radiolysis of Water on UO_2 and Other Oxides, The Journal of Physical Chemistry B, 107 (2003) 13623-13628.
[28] S. Le Caër, P. Rotureau, F. Brunet, T. Charpentier, G. Blain, J.P. Renault, J.-C. Mialocq, Radiolysis of Confined Water. 3. Hydrogen Production at High Dose Rate, Chem. Phys. Chem., 6 (2005) 2585-2596.
[29] P. Rotureau, J.P. Renault, B. Lebeau, J. Patarin, J.-C. Mialocq, Radiolysis of confined water : molecular hydrogen formation, ChemPhysChem, 6 (2005) 1316-1323.
[30] J.A. LaVerne, S.E. Tonnies, H_2 Production in the Radiolysis of Aqueous SiO_2 Suspensions and Slurries, The Journal of Physical Chemistry B, 107 (2003) 7277-7280.
[31] R. Essehli, F. Crumière, G. Blain, J. Vandenborre, F. Pottier, B. Grambow, M. Fattahi, M. Mostafavi, H_2 production by γ and He ions water radiolysis, effect of presence TiO_2 nanoparticles, International Journal of Hydrogen Energy, 36 (2011) 14342-14348.
[32] M. Alam, F. Miserque, M. Taguchi, L. Boulanger, J.P. Renault, Tuning hydrogen production during oxide irradiation through surface grafting, Journal of Materials Chemistry, 19 (2009) 4261-4267.
[33] J.A. LaVerne, L. Tandon, H_2 and Cl_2 Production in the Radiolysis of Calcium and Magnesium Chlorides and Hydroxides, The Journal of Physical Chemistry A, 109 (2005) 2861-2865.
[34] T. Zidki, H. Cohen, D. Meyerstein, D. Meisel, Effect of Silica-Supported Silver Nanoparticles on the Dihydrogen Yields from Irradiated Aqueous Solutions, The Journal of Physical Chemistry C, 111 (2007) 10461-10466.
[35] E.A. Carrasco-Flores, J.A. LaVerne, Surface species produced in the radiolysis of zirconia nanoparticles, The Journal of Chemical Physics, 127 (2007) 234703-234707.
[36] V. Wasselin-Trupin, G. Baldacchino, S. Bouffard, B. Hickel, Hydrogen peroxide yields in water radiolysis by high-energy ion beams at constant LET, Radiation Physics and Chemistry, 65 (2002) 53-61.
[37] C.M. Lousada, M. Trummer, M. Jonsson, Reactivity of H_2O_2 towards different UO_2-based materials: The relative impact of radiolysis products revisited, Journal of Nuclear Materials, In Press, Corrected Proof.

[38] A. Hiroki, J.A. LaVerne, Decomposition of Hydrogen Peroxide at Water-Ceramic Oxide Interfaces, The Journal of Physical Chemistry B, 109 (2005) 3364-3370.
[39] J.F. Ziegler, J.P. Biersack, U. Littmark, The Stopping and Range of Ions in Matter, New York, 1985.
[40] J.F. Ziegler, M.D. Ziegler, J.P. Biersack, SRIM The stopping and range of ions in matter (2010), Nuclear Instruments and Methods in Physics Research Section B: Beam Interactions with Materials and Atoms, 268 (2010) 1818-1823.
[41] H. Fricke, E.J. Hart, Chemical dosimetry, Radiation Dosimetry, Attix F.H. et Roesch W.C, New York, USA, 1966.
[42] J.A. LaVerne, R.H. Schuler, Radiation chemical studies with heavy ions: oxidation of ferrous ion in the Fricke dosimeter, The Journal of Physical Chemistry, 91 (1987) 5770-5776.
[43] M. Matsui, H. Seki, T. Karasawa, M. Imamura, Radiation Chemical Studies with Cyclotron Beams, (I) Fricke Solution, Journal of Nuclear Science and Technology, 7 (1970) 97-104.
[44] R.D. Saini, P.K. Bhattacharyya, Radiolytic oxidation of U(IV) sulphate in aqueous solution by alpha particles from cyclotron, International Journal of Radiation Applications and Instrumentation. Part C. Radiation Physics and Chemistry, 29 (1987) 375-379.
[45] A.O. Allen, C.J. Hochanadel, J.A. Ghormley, T.W. Davis, Decomposition of water and aqueous solutions under mixed fast neutron and γ radiation, The Journal of Physical Chemistry, 56 (1952) 575-586.
[46] D.L.A.d. Faria, S.V. Silva, M.T.d. Oliveira, Raman microspectroscopy of some iron oxides and oxyhydroxides, Journal of Raman Spectroscopy, 28 (1997) 873-878.
[47] S. Oh, D.C. Cook, H.E. Townsend, Characterization of Iron Oxides Commonly Formed as Corrosion Products on Steel, Hyperfine Interactions, 112 (1998) 59-66.
[48] C. Pisapia, B. Humbert, M. Chaussidon, F. Demoisson, C. Mustin, Accurate μRaman characterization of reaction products at the surface of (bio)oxidized pyrite, American Mineralogist, 95 (2010) 1730-1740.
[49] M. Bouchard, D.C. Smith, Catalogue of 45 reference Raman spectra of minerals concerning research in art history or archaeology, especially on corroded metals and coloured glass, Spectrochimica Acta Part A: Molecular and Biomolecular Spectroscopy, 59 (2003) 2247-2266.
[50] B. Pastina, J.A. LaVerne, Effect of Molecular Hydrogen on Hydrogen Peroxide in Water Radiolysis, The Journal of Physical Chemistry A, 105 (2001) 9316-9322.
[51] C.M. Lousada, M. Jonsson, Kinetics, Mechanism, and Activation Energy of H_2O_2 Decomposition on the Surface of ZrO_2, The Journal of Physical Chemistry C, 114 (2010) 11202-11208.
[52] E. Ekeroth, O. Roth, M. Jonsson, The relative impact of radiolysis products in radiation induced oxidative dissolution of UO_2, Journal of Nuclear Materials, 355 (2006) 38-46.
[53] S. Wang, H. Xin, The γ-irradiation-induced chemical change from γ-FeOOH to Fe_3O_4, Radiation Physics and Chemistry, 56 (1999) 567-572.

Figures and Tables

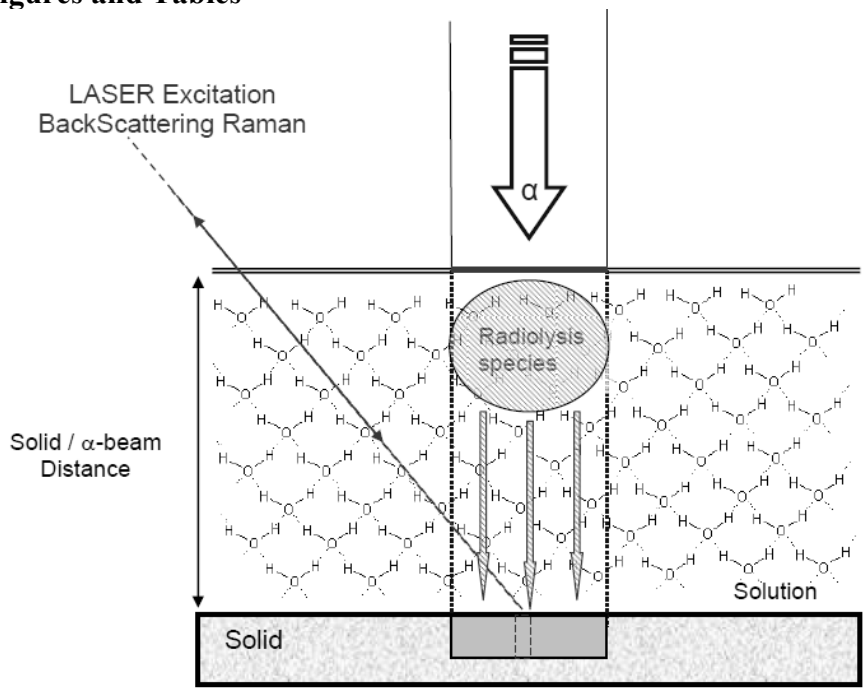

Figure 1: *In situ* Raman spectroscopic device experiment under $^{4}He^{2+}$ ions beam irradiation onto the ARRONAX facility vertical beam line (Borosilicate Glass Disc Thickness = 150 ± 10 µm, Electrolyte Thickness = 5 mm)

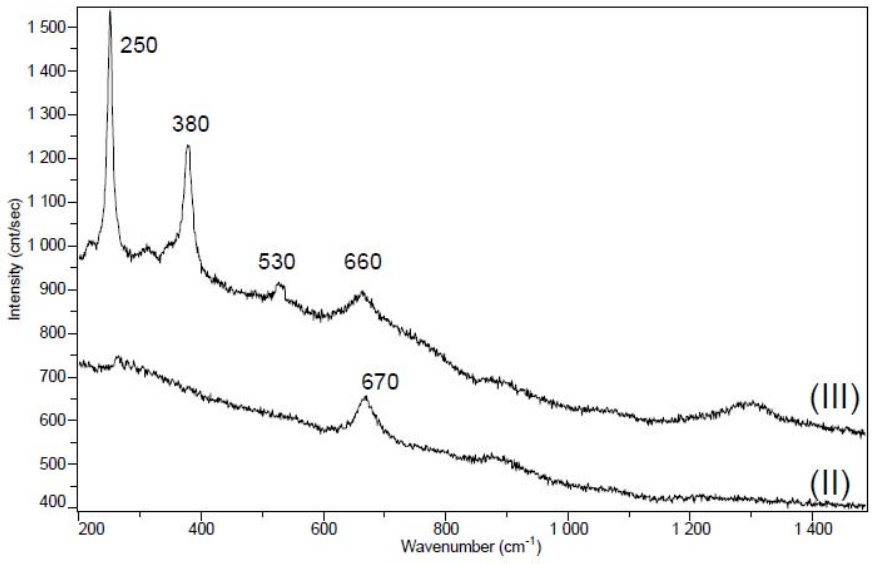

Figure 2: Corroded iron sample (set II) with Raman band of magnetite phase at 670 cm^{-1} and corroded carbon steel sample (set III) with Raman bands of lepidocrocite phase at 250/380/530/660 cm^{-1} identified in the literature [48]

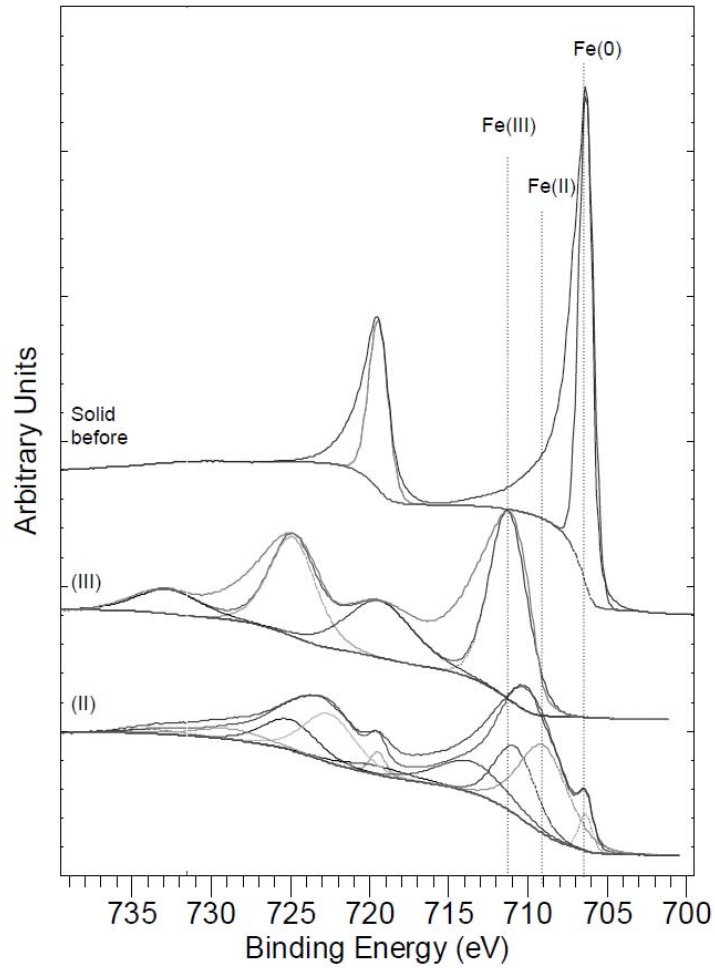

Figure 3: Fe2p XPS spectra obtained onto the two solid samples before irradiation but after the etching process with Fe(0) component, the iron sample (set II) with the Fe(II)/Fe(III) components and the carbon steel sample (set III) with the Fe(III) component (cf. Table 3)

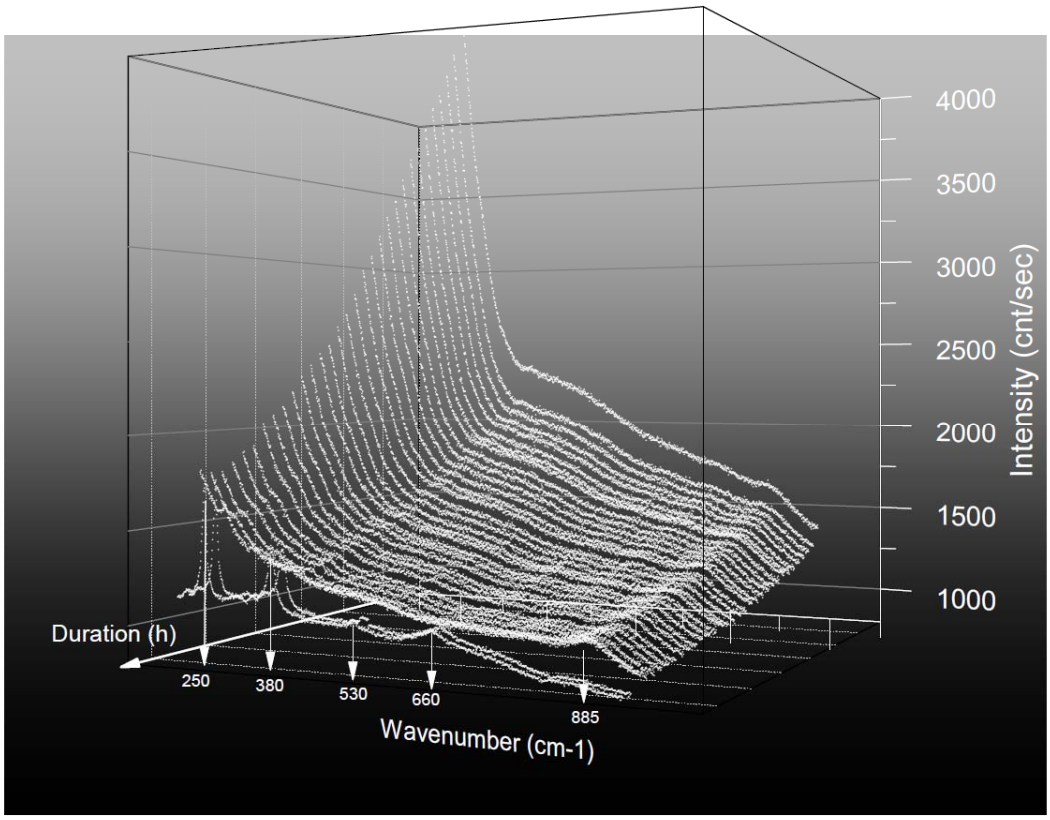

Figure 4: Raman spectra of set IV during the *in situ* experiment with an experimental time of 15 h after the irradiation. Corroded carbon steel sample with formation vs. time of the typical Raman bands of lepidocrocite phase at 250/380/530/660 cm^{-1} and H_2O_2 Raman band at 885 cm^{-1}

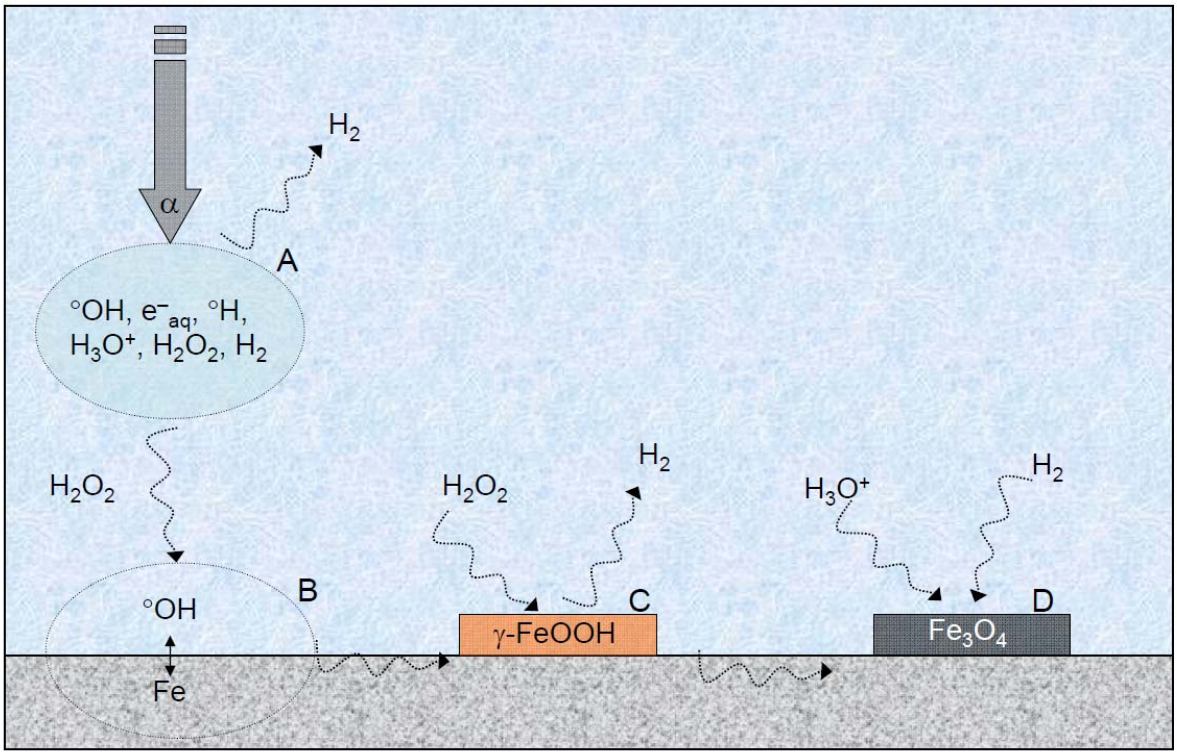

Figure 5: Scheme of iron corrosion mechanisms under $^{4}He^{2+}$ ions irradiation, (A) water radiolysis, (B) H_2O_2 catalytic decomposition and iron oxidation, (C) Lepidocrocite γ-FeOOH formation with H_2 production (carbon steel sample), (D) Magnetite Fe_3O_4 formation with H_2 consumption (pure iron sample)

Table 1: Experiments sets details used in this work with set name, solid nature, atmosphere in the irradiation cell, $^{4}He^{2+}$ irradiation experiment conditions (Energy, Time, Dose) and measurements performed

Sets	Solid	Atmosphere	Irradiation experiments			Measurement
			E(MeV)	Time(min)	Dose(kGy)	
I		Ar	5.0	15	1.2	$[H_2]$, $[H_2O_2]$
II	Iron	Ar	5.0	15	1.2	$[H_2]$, $[H_2O_2]$
II'			5.0	120	9.6	*ex situ*
III	Carbon Steel	Ar	5.0	15	1.2	$[H_2]$, $[H_2O_2]$
III'			5.0	120	9.6	*ex situ*
IV	Carbon Steel	Aerated	64.7	3	22.5	*in situ*
V	Iron	Ar				*ex situ*
VI	Carbon Steel	Ar				*ex situ*
VII	Carbon Steel	Ar/H_2	64.7	3	22.5	*in situ*
VIII	Carbon Steel	Aerated	H_2O_2 addition			*in situ*

Table 2: Chemical Composition of P235GH

Element	% by mass	Element	% by mass
Carbon (C)	≤0.16	Silicon (Si)	≤0.35
Manganese (Mn)	0.60 to 1.20	Phosphorous (P) (max)	0.025
Sulphur (S) (max)	0.015	Aluminium (Al)	≤0.020
Nitrogen (N)	≤0.012	Chromium (Cr)	≤0.30
Copper (Cu)	≤0.30	Molybdenum (Mo)	≤0.08
Niobium (Nb)	≤0.020	Nickel (Ni)	≤0.30
Titanium (Ti) (max)	0.03	Vanadium (Vi)	≤0.02

Table 3: Parameters used in order to fit the Fe2p XPS spectra for sets II and III (cf. Figure 3)

Spectra	Peak	Binding energy (eV)	FWHM (eV)	Lorentzian/ Gaussian ratio (%)
$Fe_{2p3/2}$	Fe(0)	706.9	1.1	30
	Fe(II)	709.0	3.6	30
	Fe(III)	711.3	2.8	30

Table 4: Measured concentrations for radiolytic species (H_2, H_2O_2) for sets I, II, III respectively by µ-GC, Ghormley triiodide method and pH measurements

Sets	$[H_2]$ (mol.L^{-1})	$[H_2O_2]$ (mol.L^{-1})
I	$1.0\pm0.1\ 10^{-4}$	$7.1\pm0.7\ 10^{-5}$
II	$0.3\pm0.1\ 10^{-4}$	$5.9\pm0.6\ 10^{-5}$
III	$1.6\pm0.2\ 10^{-4}$	$6.3\pm0.6\ 10^{-5}$

Table 5: Corrosion products, XPS components and Raman shift for each experiment set

Sets	Raman shift (cm^{-1})	XPS components	Corrosion products
II	670	Fe(II)/Fe(III)	Magnetite
III	250/380/530/660	Fe(III)	Lepidocrocite
IV	250/380/530/660	Fe(III)	Lepidocrocite
V	No Band	Fe(0)	Initial
VI	No Band	Fe(0)	Initial
VII	No Band	Fe(0)	Initial
VIII	250/380/530/660	Fe(III)	Lepidocrocite